The Two Emission States of PSR B1534+12

S. Q. Wang[1,2,3,4] , G. Hobbs[3], J. B. Wang[1,5,6] , R. Manchester[3] , N. Wang[1,5,6] , S. B. Zhang[2,3,7], Y. Feng[2,3,8] ,
W.-Y. Wang[2,9], D. Li[2,8,10] , S. Dai[3], K. J. Lee[11], S. J. Dang[1,2,12], and L. Zhang[2,3,8]

[1] Xinjiang Astronomical Observatory, Chinese Academy of Sciences, 150 Science 1-Street, Urumqi, Xinjiang 830011, People's Republic of China;
wangjingbo@xao.ac.cn
[2] University of Chinese Academy of Sciences, Beijing 100049, People's Republic of China
[3] CSIRO Astronomy and Space Science, P.O. Box 76, Epping, NSW 1710, Australia
[4] CAS Key Laboratory of FAST, NAOC, Chinese Academy of Sciences, Beijing 100101, People's Republic of China
[5] Key Laboratory of Radio Astronomy, Chinese Academy of Sciences, 150 Science 1-Street, Urumqi, Xinjiang, 830011, People's Republic of China
[6] Xinjiang Key Laboratory of Radio Astrophysics, 150 Science1-Street, Urumqi, Xinjiang, 830011, People's Republic of China
[7] Purple Mountain Observatory, Chinese Academy of Sciences, Nanjing 210008, People's Republic of China
[8] National Astronomical Observatories, Chinese Academy of Sciences, A20 Datun Road, Chaoyang District, Beijing 100101, People's Republic of China
[9] Key Laboratory for Computational Astrophysics, National Astronomical Observatories, Chinese Academy of Sciences, 20A Datun Road, Beijing 100101, People's Republic of China
[10] NAOC-UKZN Computational Astrophysics Centre, University of KwaZulu-Natal, Durban 4000, South Africa
[11] Kavli Institute for Astronomy and Astrophysics, Peking University, Beijing 100871, People's Republic of China
[12] School of Physics and Electronic Science, Guizhou Normal University, Guiyang, 550001, People's Republic of China

Abstract

We have observed PSR B1534+12 (J1537+1155), a pulsar with a neutron star companion, using the Five-hundred-meter Aperture Spherical radio Telescope. We found that this pulsar shows two distinct emission states: a weak state with a wide pulse profile and a burst state with a narrow pulse profile. The weak state is always present. We cannot, with our current data, determine whether the pulse energy of the weak state follows a normal or a log-normal distribution. The burst state energy distribution follows a power law. The amplitude of the single-pulse emission in the burst state varies significantly; the peak flux intensity of the brightest pulse is 334 times stronger than that of the average pulse. We also examined the timing precision achievable using only bright pulses, which showed no demonstrable improvement because of pulse jitter and therefore quantified the jitter noise level for this pulsar.

1. Introduction

Pulsars are fast-rotating and highly magnetized neutron stars. They exhibit diverse emission properties. For instance, pulsars can suddenly switch off (known as pulse nulling or intermittency; e.g., Backer 1970) or their profile can discretely change (known as pulse mode changing; e.g., Bartel et al. 1982). The nulling timescale is typically in the range of several pulse periods to hours (Wang et al. 2007), whereas the intermittency timescale is from many days to years (Kramer et al. 2006; Wang et al. 2020). Observed links between the nulling and mode changing phenomena suggest that they are the two manifestations of the same phenomenon (Wang et al. 2007). To date, both nulling and mode changing have been detected in more than 200 normal pulsars.

A single pulse for some pulsars can be tens or hundreds of times brighter than the average pulse. This rare phenomenon is known as a giant pulse and such pulses have been detected in 16 pulsars: 11 normal pulsars and five millisecond pulsars (Ershov & Kuzmin 2003; Hankins et al. 2003; Johnston & Romani 2003; Kuzmin & Ershov 2004; Soglasnov et al. 2004; Knight et al. 2005; Kuzmin & Ershov 2006; Tsai et al. 2015). The giant pulses are often associated with high-energy emission (Romani & Johnston 2001). The pulse energy for the giant pulses generally follows a power-law distribution in contrast to the pulse energy for normal pulses, which follows a normal or log-normal distribution (Karuppusamy et al. 2010; Mickaliger et al. 2018). A similar phenomenon is the giant micropulses, in which the flux density is significantly greater

than typical value at specific pulse phases, but the overall integrated flux density of the profile remains approximately constant (Kramer et al. 2002). This phenomenon has been detected in some young pulsars, such as the Vela pulsar (Kramer et al. 2002), PSR B1706−44 (Johnston & Romani 2002), and PSR J0901−4624 (Raithel et al. 2015). The energy density of these micropulses also follow a power-law distribution.

The single-pulse variations influence the timing precision achievable for a given pulsar (Cordes & Shannon 2010; Shannon et al. 2014) and provide a fundamental limit on the achievable timing precision on a short timescale. This is known as "pulse jitter."

PSR B1534+12 is a millisecond pulsar with a 37.9 ms period in orbit with a neutron star companion with a 10.1 hr orbital period. This pulsar was discovered using the Arecibo 305 m radio telescope in the 430 MHz band (Wolszczan 1991). Timing analysis of this pulsar has produced precise measurements of five post-Keplerian parameters, making it valuable in testing gravitational theories (Stairs et al. 2002; Fonseca et al. 2014). Sallmen & Backer (1995) described the single-pulse statistics for this pulsar at 430 MHz using the Arecibo telescope and detected a few narrow single pulses with a characteristic width of ∼160 μs (see also Sallmen 1998). PSR B1534+12 is the first double neutron star binary pulsar that shows this phenomenon.

In this Letter we have continued this earlier work, but with the highly sensitive Five-hundred-meter Aperture Spherical
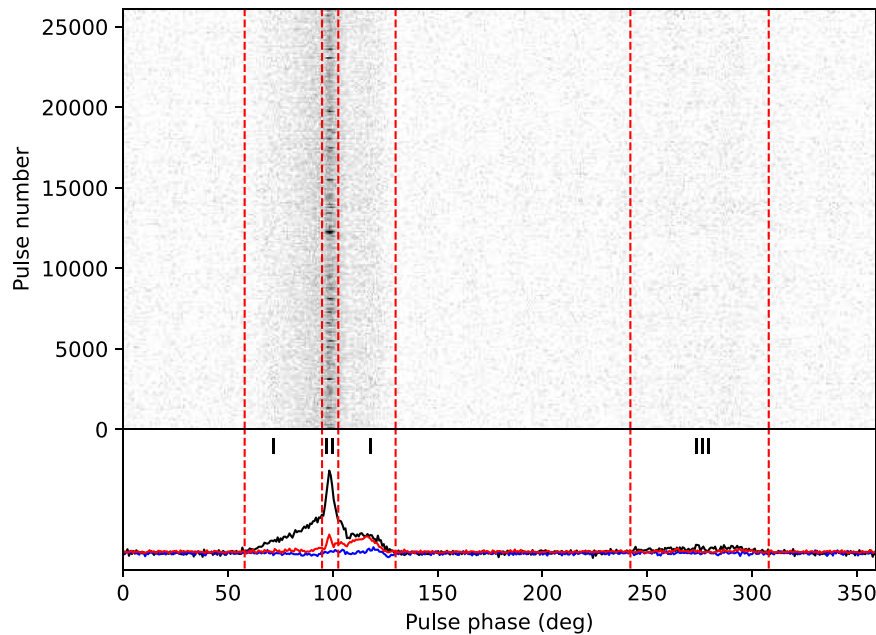
Figure 1. Individual pulses sequence and the accumulated pulse profiles for PSR B1534+12. The average pulse profile is shown in the bottom panel. The main pulse is divided into two components by the vertical red dashed lines, labeled "I" and "II." The interpulse is labeled as "III."

radio telescope (FAST; Nan et al. 2011) radio telescope. In Section 2 of this Letter, we describe our observation of PSR B1534+12. In Section 3, we present our analysis of the single pulses detected during this observation. We summarize our results in Section 4.

2. Observations and Data Processing

FAST is equipped with an *L*-band array of 19 feed horns (Li et al. 2018) that covers 1.05–1.45 GHz and was installed in 2018 May (Jiang et al. 2019). In this work, the central beam of that receiver was used to observe PSR B1534+12 on 2019 July 27 for 16 minutes. A total of 26,115 pulses were obtained during that observation with a time resolution of 49.152 μs and a channel bandwidth of 0.122 MHz. The data were recorded in a search mode PSRFITS file (Hotan et al. 2004).

To analyze the data set, we used DSPSR (Hotan et al. 2004) to extract individual pulses according to the timing ephemeris provided by the pulsar catalog (PSRCAT; Manchester et al. 2005); note that we use the -K option in DSPSR, which removes the inter-channel dispersion delays.[13] We averaged the time samples to produce 512 phase bins for each pulse profile. The observation was affected by radio-frequency interference (RFI). We first automatically flagged the RFI and removed 5% of the band-edges using the PSRCHIVE software package (Hotan et al. 2004). We completed the RFI flagging using the interactive software package PAZI that allowed us to identify any remaining frequency channels affected by RFI. In total we removed 1186 frequency channels corresponding to 29% of the total. Further details of the RFI environment around FAST are provided in Section 6 of Jiang et al. (2019).

Calibration files, in which a switched calibrator source was used, were also recorded and subsequently folded at the calibration pulse period of 2.01326592 s. The pulsar observation was subsequently calibrated using the PSRCHIVE program

PAC to flatten the bandpass and to transform the polarization products to Stokes parameters. Topocentric times of arrival (ToAs) were obtained by cross correlating the mean pulse profile with a noise-free template using PSRCHIVE. Timing residuals were formed using the TEMPO2 software package (Hobbs et al. 2006).

3. Results

3.1. The Two Emission States

The 26115 individual pulses in our observation of PSR B1534+12 is shown in the top panel of Figure 1 as a grayscale image. We also display a pulse stack containing 10 adjacent individual pulses, shown in Figure 2.

The pulse profile can be divided into three components: two in the main pulse and the interpulse. A "weak emission" region is labeled as "I" in the bottom panel of Figure 1. A narrower, brighter component is labeled as "II" (note that region "II" does not include region "I"). The interpulse is labeled as "III."

As seen in Figures 1 and 2, the intensity in region "II" is highly variable, and we call this "burst emission." The weak state is always present. When both exist, then the two states overlap. To identify whether the burst state exists in any particular pulse, we determine the signal-to-noise ratio (S/N) as $I_{\mathrm{peak}}/\sigma_{\mathrm{off}}$, where I_{peak} is the peak intensity of a single pulse in the region "II" and σ_{off} is the rms of the off-pulse region. If the S/N for a single pulse is larger than 5σ, then we initially classify it as likely being in the burst state. We subsequently check every single pulse in this selection of pulses to confirm our classification. In total 443 single pulses in the burst state were obtained using this method. For pulses with the S/N smaller than 3σ, we classify the pulse as belonging to the weak state. Between 3σ and 5σ, we do not attempt to classify the state.

To determine the pulse-energy distributions we calculate the area (in non-physical units) across the regions "I" and "II" for the weak pulse and the regions "II" for the burst pulse, respectively. We also calculate the area in an off-pulse region.

---

[13] FAST does not have the signal processing capability to provide coherently dedispersed search mode data streams. The dispersive delay for the pulsar across a single frequency channel of 0.122 MHz is 6 μs.
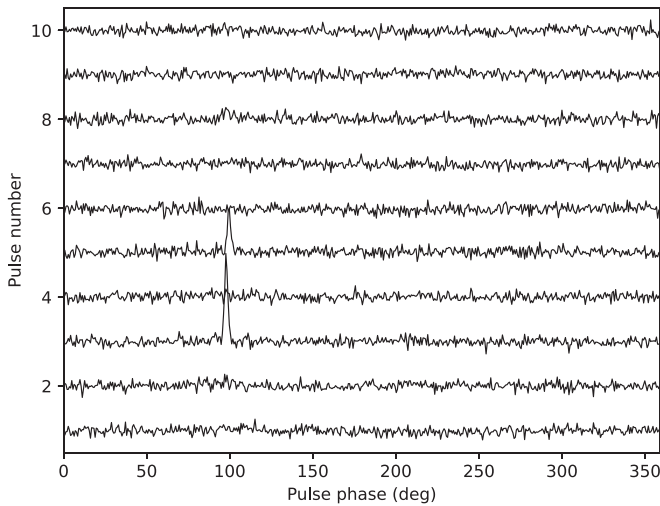
Figure 2. Single-pulse stack of 10 single pulses for PSR B1534+12.

We normalize each pulse by the mean value in the on-pulse region. The results are shown in Figure 3. The noise in the off-pulse region (solid red line) follows the expected normal distribution. For many of the pulses in the weak state, we cannot distinguish them from the off-pulse noise, but there is a significant excess at high energies and we fit this both with normal+normal and normal+log-normal distributions. The two fits are almost identical, and therefore we cannot distinguish between a normal or a log-normal distribution for the weak state pulses. The blue histogram shows the distribution of the burst emission and we model that using a power-law distribution with a power-law exponent of -2.06 ± 0.05.

The emission from this pulsar at 430 MHz has a similar energy distribution (see Figure 1 in Sallmen & Backer 1995). However, the single-pulse energy in our observation extended out to about 38 times the average pulse energy, which is much large than reported in the earlier paper at 430 MHz (which extended to $\sim$13 times the average pulse energy).

The average pulse profiles of the two emission states are shown in the top and bottom panels of Figure 4. We do not observe any increase in the strength of the interpulse during a burst state. The pulse emission for weak state is always present. The pulse profile for the burst emission can be obtained by subtracting the average profile of the weak state from the burst profile. This is shown in the bottom panel of Figure 4. This burst emission is much narrower than that for the weak state. The FWHM (W50) of the profiles are 0.35 ms and 3.78 ms, respectively. To form the polarization profiles we used the cataloged rotation measure for this pulsar of 10.6 ± 2 rad m^{-2} (Weisberg et al. 2004).[14]

Arzoumanian et al. (1996) showed, by fitting the rotating-vector model, that this pulsar is nearly an orthogonal rotator. However, the polarization properties of the two emission states differ. The linear and circular polarization are shown in Figure 4 as red and blue lines, respectively. The position angle of the linear polarization is shown in the upper sub-panels for each plot. The position angle difference between the two states ranges from $56°$ to $91°$ across the burst-state profile. In the weak state, the linearly polarized intensity increases gradually

---

[14] We also used our own data to determine the rotation measure and obtained 10 ± 13 rad m^{-2}. This is not unexpected because we are only using the 16 minutes data, which provides a S/N of the profile of 137.9. This value is consistent, but has a much larger uncertainty than the cataloged value.
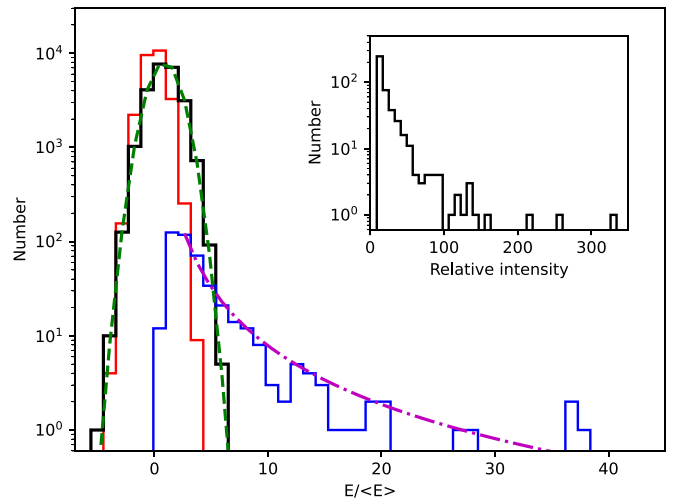

Figure 3. Pulse-energy histograms for the off-pulse region (solid red line), weak state (solid black line) and burst state (solid blue line) for PSR B1534+12. The pulse energies are normalized by the mean on-pulse energy. The green dashed line is noise and weak state distribution. The magenta dashed–dotted line is power-law distribution fitted to the burst states. The distribution of the relative peak flux intensity compared to the average pulse for the pulses in the burst state is shown in the inner plot.
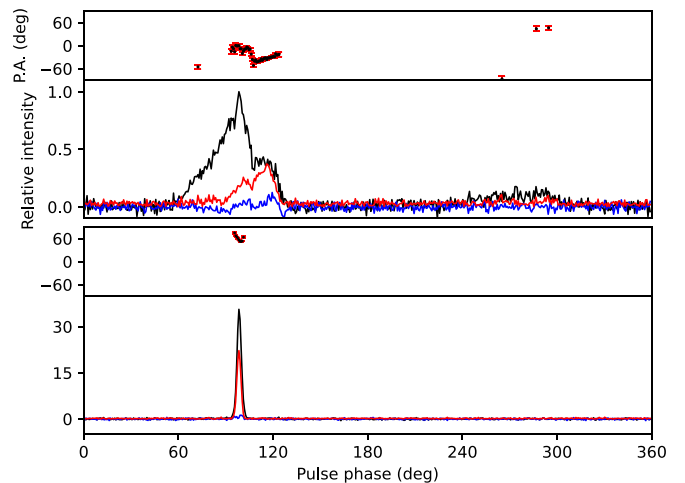

Figure 4. Polarization profiles for PSR B1534+12 in the weak (top panel) and burst states (bottom panel). The position angle (black dots) and corresponding uncertainties (red bars) of the linearly polarized emission are shown as a function of pulse phase. The black, red, and blue lines are for the total intensity, linearly polarized intensity, and circularly polarized intensity, respectively. All pulse profiles are normalized by the average profile for the weak state.

over the pulse phase. It is low in the leading pulse component, whereas it becomes much higher (about 85%) in the trailing component of the main pulse. In the burst state, the linearly polarized intensity is about 62% of total intensity.

For single pulses in the burst state, the peak flux intensities are in the range 9–334 times stronger than the peak flux intensity averaged over all pulses (see the inner plot in Figure 3). These bright pulses are generated in a narrow phase range, and have W50 pulse widths in the range of 49 to 674 μs (the characteristic width of these bright pulses at 430 MHz is $\sim$160 μs; Sallmen & Backer 1995). We also analyzed the polarization profile of the brightest single pulse. The fractional linear polarization is high (83% at the peak) and significant circular polarization is detected (18% at its maximum value).
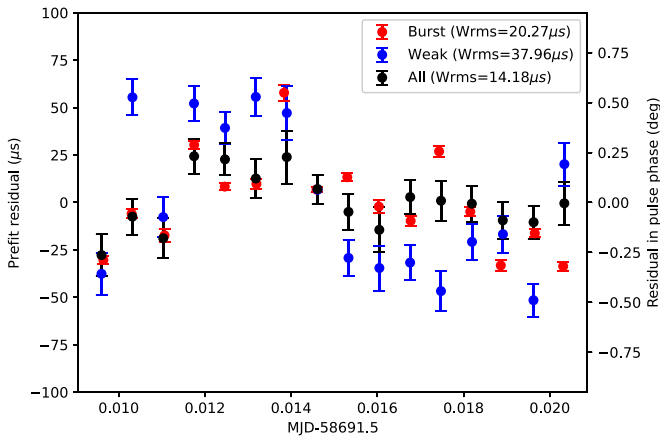
Figure 5. Timing residuals for the average pulse profiles formed by the pulses in burst state (red dots), weak state (blue dots), and all the pulses together (black dots). The bars give the ToA uncertainties. The weighted rms residuals are listed in the Figure legend. The mean ToA uncertainties are 2.5, 32.2 and 10.1 μs, respectively.

3.2. Timing the Brightest Pulses

Our results show that the brighter pulses are generated in a narrow pulse phase range. This suggests that that it may be possible to improve the timing precision (at least over short timescales) if only the brightest pulses are selected. To study this, we divided the observation into 16 segments each of ~1 minute duration and, within each segment, summed separately all the pulses, as well as those only in the burst state (S/N > 5) and those only in the weak state (S/N < 3). Three analytic pulse templates were formed from these summed profiles.

We formed pulse ToA by cross correlating these resulting summed profiles using the relevant standard template. We then formed timing residuals using the timing model provided by the online pulsar catalog (Manchester et al. 2005). The timing residuals for the burst state, weak state, and for all the single pulses are shown in Figure 5. As expected, the ToA uncertainties were smaller for the pulses in the burst state. However, the timing residuals for the burst state scatter by significantly more than their uncertainties. We quantify this jitter as the quadrature difference between the observed rms residual and the rms ToA uncertainty, $\sigma_J^2(N_p) = \sigma_{obs}^2(N_p) - \sigma_{ToA}^2(N_p)$ where N_p is the number of pulses that have been averaged together. Our results are shown in Figure 6 and the rms noise caused by this jitter per pulse, $\sigma_J(1) = 62 \mu$s.

4. Discussions and Conclusions

We have presented single-pulse profiles for PSR B1534+12. The emission from this pulsar shows two different states: a weak state with a wide pulse profile and a burst state with a narrow pulse profile. This phenomenon has never been seen in double neutron star systems before, but emission state changes like this have been observed in young pulsars (Weltevrede et al. 2006). We note that this phenomenon is not like the typical mode changing, which the pulsar emission switches between two or more stable states (Bartel et al. 1982). For PSR B1534 +12, the weak emission is always present in our observation, while the burst emission appears in conjunction with the weak state, but only in a narrow pulse phase. These results suggest that the emission for the two states is generated in two different regions in the pulsar magnetosphere. This is evidenced by their
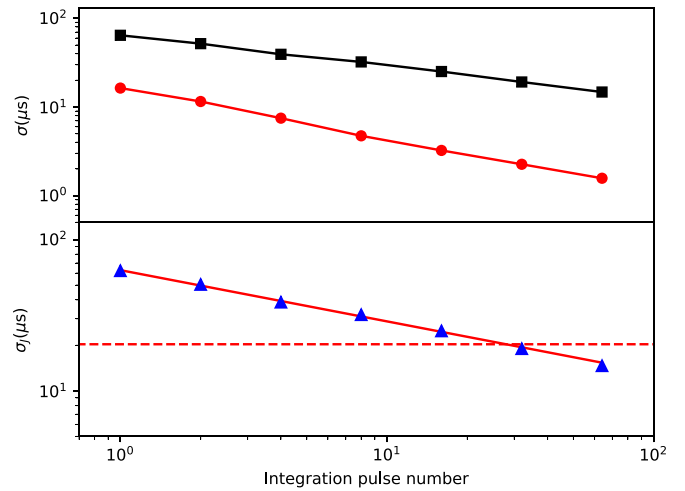

Figure 6. Determination of the jitter noise in PSR B1534+12. Top panel: the rms residuals vs. the number of pulses averaged (N_p) (squares) and the average ToA uncertainties (circles). Bottom panel: the variations for $\sigma_J(N_p)$ vs. N_p. The red line is the best fitting model for the jitter noise with the index of -0.35 ± 0.01. The dashed line is for the weighted rms residual of 20.27 μs.

different observation properties both in pulse-energy distributions and polarization properties. Further multi-frequency observations (with instruments such as the Parkes ultra-wide-bandwidth receiver; see Hobbs et al. 2020) are needed to further constrain the emission geometry of these regions.

During the burst state we identified bright pulses that are similar to those defined as giant pulses. The bright state pulses follow a power-law distribution, which is the same as the pulse-energy distribution for giant pulses (Johnston & Romani 2003; Karuppusamy et al. 2010). However, this power-law distribution is detectable to relatively low pulse energies. Pulsars that exhibit giant pulses are divided into two classes based on the magnetic field in the light cylinder B_{LC}. For the first class, this is ~10^6 G, and that of the second class is from 10 to 100 G (Kuzmin & Ershov 2004). The typical pulse width for the first class is measured in microseconds or even nanoseconds. The typical widths for the second class are several milliseconds. The pulse widths of the bright pulses of PSR B1534+12 lie in the range of several tens to several hundred microseconds, which is between the typical pulse width of the two giant pulses classes. The B_{LC} of PSR B1534+12 is about 1.67×10^3 G and also falls into the gap between these classes. This pulsar provides evidence for connection between the two giant pulse classes.

The bright pulses in the pulsar share some similar properties to the giant pulses of PSR B1937+21. For instance, they are all generated in a narrow phase range. However, the typical pulse width for the bright pulses in PSR B1534+12 is much wider (the giant pulses for PSR B1937+21 are typically a few hundred nanoseconds wide; McKee et al. 2019). The bright pulses in PSR B1534+12 exhibit strong linear polarization, whereas the giant pulses of PSR B1937+21 are almost 100% circularly polarized (Soglasnov et al. 2004).

The pulses in the burst state for PSR B1534+12 share some properties with the giant micropulses. For instance, they follow power-law distributions and have the similar pulse widths. However, they are different. First, the giant micropulse is typically seen in young pulsars (Johnston & Romani 2002), while PSR B1534+12 is a partly recycled pulsar. Second, the

giant micropulse is a separate component of a single pulse, which may be caused by microbeams and some are quasi-periodic (Kramer et al. 2002). For PSR B1534+12, our results suggest that the bright pulse emission is generated in a different region in the pulsar magnetosphere compared with the weak emission, which is always present.

Pulsars like PSR B1534+12 can be used to study fundamental physics such as theories of gravity. Therefore, they deserve detailed studies of their emission properties and how those properties may affect the long-term timing campaigns. We studied the timing precision achievable for PSR B1534+12 using the bright pulses and found that even though the ToA uncertainties decrease significantly when only these bright and narrow pulses are selected, the rms timing residuals (and hence the precision achievable for any relativistic study) for PSR B1534+12 does not improve. This is not unexpected as many pulsars exhibit jitter, e.g., PSR J0437−4715 (Liu et al. 2012), PSR J1713+0747 (Shannon & Cordes 2012), and PSR J1022+1001 (Liu et al. 2015), and this is a major limitation of high-precision pulsar timing experiments with sensitive telescopes (see, e.g., Hobbs et al. 2019; Li et al. 2019).

We will continue to monitor this pulsar with FAST and expect that our results will provide more information on the single-pulse statistics of this pulsar as well as the long-term timing behavior.

ORCID iDs

S. Q. Wang ⓘ https://orcid.org/0000-0003-4498-6070
J. B. Wang ⓘ https://orcid.org/0000-0001-9782-1603
R. Manchester ⓘ https://orcid.org/0000-0001-9445-5732
N. Wang ⓘ https://orcid.org/0000-0002-1662-7700
Y. Feng ⓘ https://orcid.org/0000-0002-0475-7479
D. Li ⓘ https://orcid.org/0000-0003-3010-7661
S. Dai ⓘ https://orcid.org/0000-0002-9618-2499
L. Zhang ⓘ https://orcid.org/0000-0001-8539-4237

References

Arzoumanian, Z., Phillips, J. A., Taylor, J. H., et al. 1996, ApJ, 470, 1111
Backer, D. C. 1970, Natur, 228, 42
Bartel, N., Morris, D., Sieber, W., et al. 1982, ApJ, 258, 776
Cordes, J. M., & Shannon, R. M. 2010, arXiv:1010.3785
Ershov, A. A., & Kuzmin, A. D. 2003, AstL, 29, 91
Fonseca, E., Stairs, I. H., & Thorsett, S. E. 2014, ApJ, 787, 82
Hankins, T. H., Kern, J. S., Weatherall, J. C., et al. 2003, Natur, 422, 141
Hobbs, G., Dai, S., Manchester, R. N., et al. 2019, RAA, 19, 020
Hobbs, G., Manchester, R. N., Dunning, A., et al. 2020, PASA, 37, e012
Hobbs, G. B., Edwards, R. T., & Manchester, R. N. 2006, MNRAS, 369, 655
Hotan, A. W., van Straten, W., & Manchester, R. N. 2004, PASA, 21, 302
Jiang, P., Yue, Y., Gan, H., et al. 2019, SCPMA, 62, 959502
Johnston, S., & Romani, R. W. 2002, MNRAS, 332, 109
Johnston, S., & Romani, R. W. 2003, ApJL, 590, L95
Karuppusamy, R., Stappers, B. W., & van Straten, W. 2010, A&A, 515, A36
Knight, H. S., Bailes, M., Manchester, R. N., et al. 2005, ApJ, 625, 951
Kramer, M., Johnston, S., & van Straten, W. 2002, MNRAS, 334, 523
Kramer, M., Lyne, A. G., O'Brien, J. T., et al. 2006, Sci, 312, 549
Kuzmin, A. D., & Ershov, A. A. 2004, A&A, 427, 575
Kuzmin, A. D., & Ershov, A. A. 2006, AstL, 32, 583
Li, D., Dickey, J. M., & Liu, S. 2019, RAA, 19, 016
Li, D., Wang, P., Qian, L., et al. 2018, IMMag, 19, 112
Liu, K., Karuppusamy, R., Lee, K. J., et al. 2015, MNRAS, 449, 1158
Liu, K., Keane, E. F., Lee, K. J., et al. 2012, MNRAS, 420, 361
Manchester, R. N., Hobbs, G. B., Teoh, A., et al. 2005, AJ, 129, 1993
McKee, J. W., Stappers, B. W., Bassa, C. G., et al. 2019, MNRAS, 483, 4784
Mickaliger, M. B., McEwen, A. E., McLaughlin, M. A., et al. 2018, MNRAS, 479, 5413
Nan, R., Li, D., Jin, C., et al. 2011, IJMPD, 20, 989
Raithel, C. A., Shannon, R. M., Johnston, S., et al. 2015, ApJL, 804, L18
Romani, R. W., & Johnston, S. 2001, ApJL, 557, L93
Sallmen, S., & Backer, D. C. 1995, in ASP Conf. Ser. 72, Millisecond Pulsars. A Decade of Surprise, ed. A. S. Fruchter, M. Tavani, & D. C. Backer (San Francisco, CA: ASP), 340
Sallmen, S. M. 1998, PhD thesis, Univ. of California, Berkeley
Shannon, R. M., & Cordes, J. M. 2012, ApJ, 761, 64
Shannon, R. M., Osłowski, S., Dai, S., et al. 2014, MNRAS, 443, 1463
Soglasnov, V. A., Popov, M. V., Bartel, N., et al. 2004, ApJ, 616, 439
Stairs, I. H., Thorsett, S. E., Taylor, J. H., et al. 2002, ApJ, 581, 501
Tsai, J.-W., Simonetti, J. H., Akukwe, B., et al. 2015, AJ, 149, 65
Wang, N., Manchester, R. N., & Johnston, S. 2007, MNRAS, 377, 1383
Wang, S. Q., Wang, J. B., Hobbs, G., et al. 2020, arXiv:2005.05558
Weisberg, J. M., Cordes, J. M., Kuan, B., et al. 2004, ApJS, 150, 317
Weltevrede, P., Wright, G. A. E., Stappers, B. W., et al. 2006, A&A, 458, 269
Wolszczan, A. 1991, Natur, 350, 688